Localisation and quantification of stiffness loss based on the forced vibration of a beam traversed by a quarter-car

K. Feng, A. González & M. Casero
School of Civil Engineering, University College Dublin, Dublin, Ireland

ABSTRACT: This paper proposes a method for locating and quantifying bridge damage based on the time-varying forced frequencies due to moving traffic. The vehicle-bridge coupled system is simplified using a quarter-car model and a simply supported beam. Eigenvalue analysis shows that the eigenfrequencies of the coupled system vary for different vehicle positions. If a local stiffness loss is introduced, the forced frequencies associated with the 'damage' scenario will differ from those of a reference 'healthy' scenario. The differences between both scenarios depend on the location and severity of damage as well as on the mass and frequency ratios between quarter-car and beam models. In practice, bridge acceleration due to the crossing of a vehicle can be measured and processed using a time-frequency signal processing tool to obtain instantaneous frequencies. Changes in local stiffness are determined from comparing those instantaneous frequencies with the eigenfrequencies based on the same bridge and vehicle configuration.

1 INTRODUCTION

Many bridges in Europe were built in the 1950s and are now getting close to the end of their design life. Their deterioration has been aggravated by loads higher than foreseen at the design stage (Gkoumas et al. 2019). Therefore, proactive and effective maintenance is needed for Europe's ageing transport infrastructure to ensure its safe operation during the remaining life cycle. Structural health monitoring (SHM) methods aim to meet this need via two approaches: (1) response-based methods, and (2) model-based methods (Fan & Qiao 2011).

Response-based methods, also called model-free methods, rely on the measured response from the structure only. Hence, they do not require complicated structural models, which are often difficult to calibrate on site. Amongst these methods, the extraction of mode shapes from measured accelerations is a popular technique for damage localization. A requirement for obtaining accurate mode shapes and mode shape curvatures is the installation of a high number of sensors over as many measurement locations. The latter has been addressed recently with the recording and processing of video measurements. For instance, Yang et al. (2018) extract three full-field and high-resolution mode shapes from video measurement of a structure excited by an impact hammer. However, mode shapes and their derivatives usually have a larger statistical variability than natural frequencies and damping ratios (Sun & Chang 2002). Therefore, damage severity is difficult to estimate using only response-based methods due to missing information about the bridge structure.

Compared to response-based methods, model-based methods are better suited for both locating and quantifying damage. A detailed numerical model establishes an early healthy statistical baseline of the structure, and then the model is subsequently updated to match responses measured at different points in time. Monitored responses commonly include natural frequencies, given that their acquisition through accelerometers is easy and energy efficient, i.e., one sensor may be sufficient to extract the frequency range of interest. Guan et al. (2006) propose computer-based automated analysis algorithms to locate damage and to estimate its severity from shifts in natural frequency and changes in mode shapes. The system is tested on a fibre reinforced polymer composite bridge structure. Lederman et al. (2014) use signal processing and machine learning approaches to analyse the forced vibration responses collected from a vehicle-bridge interaction (VBI) model. Natural frequency spectrum magnitudes obtained by principal component analysis are successfully used to diagnose the severity and to locate damage in a laboratory bridge model.

The natural frequency of a bridge does not only change with the magnitude of the moving load, but also with its location (Frýba 1972). Cantero & OBrien (2013) demonstrate that the variations in natural frequencies greatly depend on the vehicle-to-

structure frequency and mass ratios. Chang et al. (2014) verify, both theoretically and experimentally, that the main frequencies of a VBI system and the frequencies of the bridge system alone may differ due to the presence of a parked vehicle on the bridge. Cantero et al. (2017) measure the evolution of frequency shifts and changes in mode shape due to a truck parked in different positions of a steel girder bridge using the Continuous Wavelet Transform (CWT). In general, operational loads are typically considered to mask the underlying true dynamic features of a bridge structure, and the dynamic properties of the bridge system alone are characterized best in free vibration. Nevertheless, González et al. (2020) use eigenvalue analysis to show how forced frequencies, due to a vehicle moving on a bridge, change for a bridge in healthy and damaged conditions. Therefore, if a similar vehicle was used to obtain the forced frequencies of a bridge in two separate moments in time, their differences could potentially be exploited to assess the damage in the structure.

This paper proposes a model-based method that relies on the changes in the forced frequency associated with the first mode due to the passage of a vehicle for locating and quantifying damage. It is based on comparing a database of theoretical forced frequencies obtained from eigenvalue analysis for a wide range of damage scenarios, with the instantaneous frequencies obtained from a measured or simulated acceleration signal from a VBI model. Section 2 describes the numerical VBI model for the healthy and damaged scenarios that serves for developing the proposed method. Section 3 describes the steps involved in the application of the damage detection method. Section 4 tests the method in two scenarios where damage location and severity are determined from reconciling dynamic transient results with a database of theoretical eigenvalues. Finally, Section 5 provides conclusions and recommendations for further research.

2 VBI MODEL

2.1 *Vehicle and bridge*

The vehicle is modelled as a two degree of freedom quarter-car and the bridge is modelled as a simply supported discretized finite element beam, as shown by Figure 1.

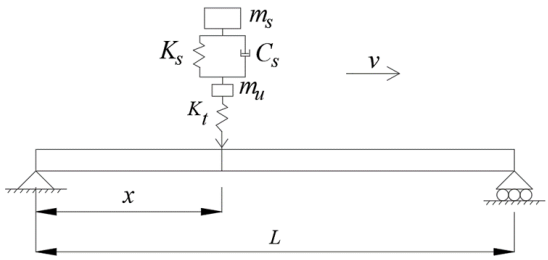

Figure 1. VBI model.

The quarter-car is composed of a sprung mass (m_s) and an unsprung mass (m_u), moving at a constant speed of 1 m/s over the beam. The unsprung mass connects to the bridge surface via a spring (K_t), while the sprung mass is connected to the unsprung mass by another spring (K_s) and a viscous damper (C_s). The values adopted for these parameters are based on Cantero & González (2008) and listed in Table 1.

Table 1. Properties of the vehicle.

Parameter	Value	Unit
Sprung mass, m_s	14×10^3	kg
Unsprung mass, m_u	1×10^3	kg
Suspension stiffness, Ks	500×10^3	N/m
Suspension damping, C_s	5×10^3	Ns/m
Tyre stiffness, K_t	3×10^6	N/m
1st Frequency, f_1	0.8495	Hz
2nd Frequency, f_2	7.9692	Hz

The beam is discretized into 150 finite beam elements 0.1 m long each. The bridge model has a total of 302 degrees of freedom (i.e., rotation and vertical displacement at both ends of each discretized elementary beam). Bridge damping is typically low and neglected here. Table 2 summarizes the values for the bridge properties.

Table 2. Properties of the bridge.

Parameter	Value	Unit
Length, L	15	m
Width, w	15	m
Depth, h	0.75	m
Mass per unit, m	28125	kg/m
2nd moment of area, I	0.5273	m^4
Modulus of elasticity, E	35×10^9	Pa
1st Frequency, f_1	5.655	Hz
2nd Frequency, f_2	22.622	Hz
3rd Frequency, f_3	50.900	Hz

By merging those degrees of freedom that vehicle and bridge have in common, the 2×2 stiffness matrix of the quarter-car and the 302×302 stiffness matrix of the finite element beam are combined into one 304×304 global stiffness matrix that varies with the

position of the vehicle. The individual mass matrices of the quarter-car and beam are also combined into one 304×304 global mass matrix that is constant in time. The coupled equations of motion are integrated to obtain the acceleration response at midspan as described by González (2010). Figure 2 shows the acceleration response for the case of a healthy condition where all beam elements maintain the stiffness values defined in Table 1.

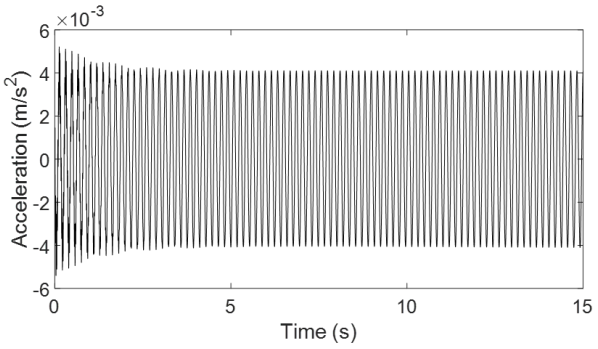

Figure 2. Acceleration response due to VBI model.

2.2 *Modelling of damage*

Various approaches for crack modelling are available in the literature. The stiffness reduction associated with a single crack, as proposed by Sinha et al. (2002), is adopted in this paper. Figure 3 shows the representative parameters for modelling a crack located at 4 m from the first beam support. The damaged depth, h_d, takes a value of $h_d = \lambda h$, where λ represents the damage level, typically given as a percentage of the total beam depth h. Following Sinha's approach, the total length affected by damage, denoted by $2l_d$ in the figure, covers a region equal to $1.5h$ at either side of the crack. In this region, the stiffness loss varies linearly until reaching a maximum loss at the crack location.

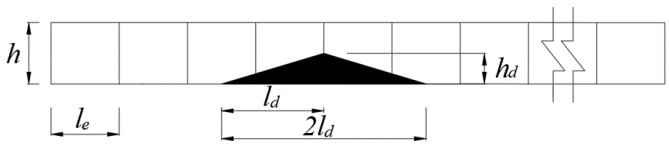

Figure 3. Crack details.

Figure 4 shows the stiffness distribution throughout the beam for crack depths that vary from λ = 0% to λ = 30% of the beam depth. When analysing a specific damage scenario, the stiffness of the beam elements affected by the crack will be modified accordingly.

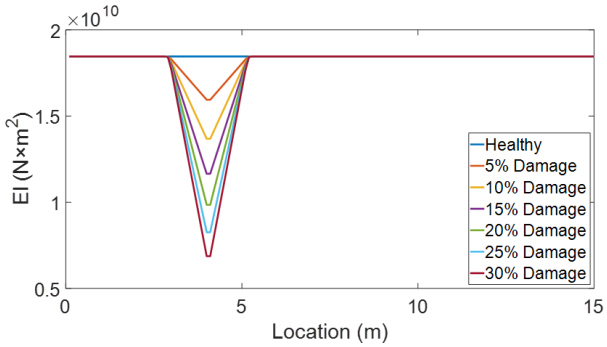

Figure 4. Stiffness profiles for 7 beams with different damage levels at location x = 4 m.

3 DAMAGE DETECTION METHOD

3.1 *Description*

Firstly, the theoretical curves of forced frequencies versus vehicle position are obtained using eigenvalue analysis for a healthy condition and multiple damage scenarios. For each damage scenario, the differences between frequencies in the damaged and healthy conditions are computed and stored in a database.

Secondly, a dynamic transient analysis of the acceleration response of the beam due to a moving load is carried out for two moments in time: an initial time from the past in which the structure is assumed to be healthy, and a time in the future when the structure has an unknown health status. The short-time Fourier transform (STFT) is employed to obtain a time-history of instantaneous forced frequencies, although alternative time-frequency techniques such as the CWT and the Hilbert-Huang transform could have also been employed.

Finally, the differences between the instantaneous forced frequencies versus vehicle position in the healthy and unknown status conditions are compared to the theoretical curves derived from eigenvalue analysis for locating and quantifying damage. Due to the symmetry of the frequency response, there are cases with two potential solutions, one to the left of the bridge centreline and another in the symmetric location to the right of the bridge centreline. The latter is overcome by comparing not only the magnitude of the differences between STFT and eigenvalue curves but also the shapes of these curves. This paper assumes that the same vehicle is employed to obtain forced frequencies for all scenarios. When implementing the algorithm in the field, a weigh-in-motion system can be used to select the forced responses corresponding to those vehicles with similar configuration and weights to that employed in the theoretical eigenvalue analysis.

3.2 *Eigenvalue analysis*

In eigenvalue analysis, the inverse of the global mass matrix is multiplied by the global stiffness matrix to obtain the eigenfrequencies of the system. It is then possible to calculate the differences in forced frequencies versus vehicle position between a damage scenario and the healthy scenario, as per Equation (1), for different damage locations and severities.

$$\{f_{diff}^{i}\} = \{f_h\} - \{f_{dmg}^{i}\} \tag{1}$$

where $\{f_h\}$ is the vector defining the forced frequencies for the healthy case, $\{f_{dmg}^{i}\}$ is the vector defining the forced frequencies for the damaged case, and $\{f_{diff}^{i}\}$ is the difference between the vectors $\{f_{dmg}^{i}\}$ and $\{f_h\}$. The parameter i represents the damage scenario number, and it ranges from 1 to 84 to cover 12 damage locations spaced by 1 m (from 2 m to 13 m from the first support), and 7 different damage levels for each location (λ = 0%, 5%, 10%, 15%, 20%, 25% and 30%). Figure 5 plots $\{f_{diff}^{i}\}$ for a damage case with λ = 15% and all analysed locations. The vertical red dash-dot line in each subfigure signals the damage location.

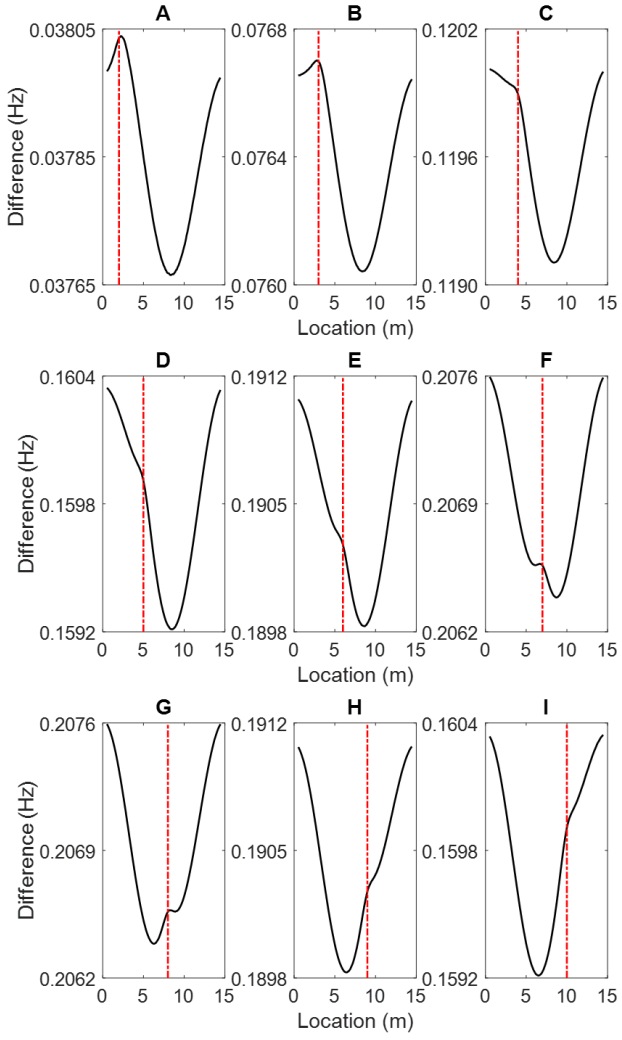

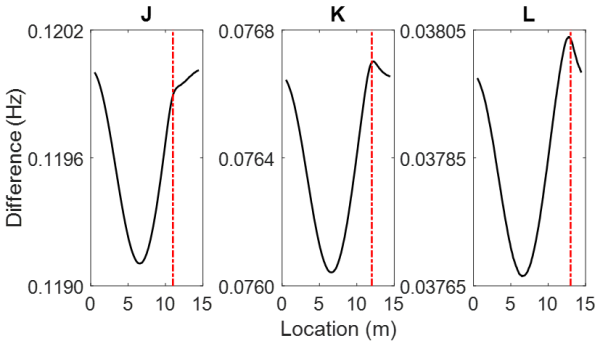

Figure 5. Difference between forced eigenfrequencies for a 15% damage located at *x* = : (A) 2 m, (B) 3 m, (C) 4 m, (D) 5 m, (E) 6 m, (F) 7 m, (G) 8 m, (H) 9 m, (I) 10 m, (J) 11 m, (K) 12 m, (L) 13 m.

Peaks are clearly seen for damages located at 2, 3, 12, and 13 m from the first support, while a change in curvature is appreciated for other damage locations. Symmetry is observed with respect to the beam midspan, i.e., between the sub-figures corresponding to *x* = 2 m (A) and *x* = 13 m (L), and between figures corresponding to *x* = 3 m (B) and *x* = 12 m (K). Further on, it will be seen how this symmetry can apparently lead to two optimal solutions.

3.3 *Dynamic transient analysis*

For the dynamic transient analysis, the equations of motion of the vehicle-bridge system are integrated to obtain a time series of the acceleration response at midspan due to the passing of the vehicle. Instantaneous frequencies need to be obtained next. The fast Fourier transform (FFT) converts time-series signals into a frequency domain representation in which the main frequencies of a structure are easily identified, but the FFT cannot depict the frequency changes over the time domain. To overcome this limitation, STFT has been proposed for providing a representation of the signal in the time-frequency domain. The STFT divides a measured response into shorter segments of the same window length and then applies the FFT to each segment separately for deriving each frequency component. Therefore, those components contain frequency changes over time. The STFT is restricted by the selection of the window width, which leads to a trade-off between frequency resolution and time resolution. In other words, a large window length will provide good resolution in the frequency domain and poor resolution in the time domain, and vice-versa (Amezquita-Sanchez & Adeli 2016).

Figures 6a and 6b show the time-frequency spectrum obtained by applying STFT to the acceleration in forced vibration provided in Figure 2. Here, the window length is set at 2^{10} samples and the hop size, at 2^5 samples. An instantaneous frequency around the first frequency of the bridge, i.e., 5.65 Hz, is

identified in Figure 6a. Figure 6b zooms into the frequency range of interest to highlight the slight changes in the first frequency as the vehicle moves along the bridge.

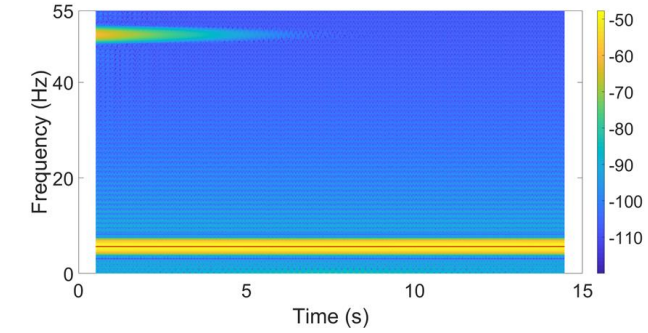

Figure 6a. Frequency-time spectrum by STFT.

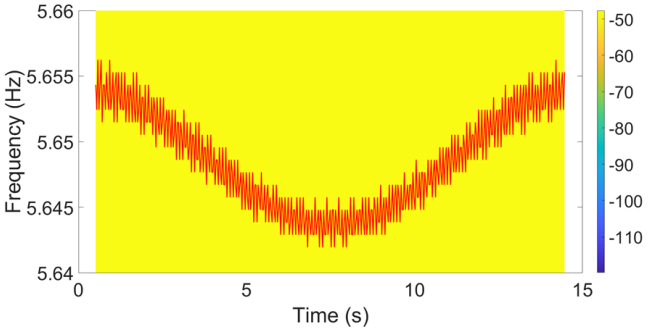

Figure 6b. Variation of the first frequency of the bridge with vehicle location.

Figure 7 shows how the curve obtained from applying STFT compares to the expected frequency change from eigenvalue analysis. The blue dashed line represents the forced frequency by eigenvalue analysis, and the solid red line represents the forced frequencies by transient analysis shown in Figure 6b. Additionally, the horizontal dash-dot black line represents the value of the frequency in free vibration, given as a reference. It can be seen that there is a good agreement between the results from the STFT and the eigenvalue analysis, although the former slightly over predicts the change in frequency and the latter is smoother. Nonetheless, the STFT appears to be a valid tool for capturing the main changes in forced frequency identified by eigenvalue analysis in the response under investigation.

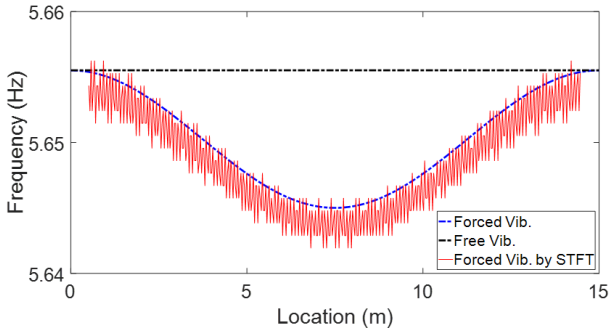

Figure 7. Variation of forced frequency with vehicle location.

3.4 *Localization and quantification of damage*

Similar to Equation (1), the difference between an 'unknown-health status' and the healthy bridge can be computed from the transient analysis by applying the STFT to the acceleration signal, as per Equation (2).

$$\{f^*_{diff}\} = \{f^*_h\} - \{f^*_{unk}\} \tag{2}$$

where $\{f^*_h\}$ is a vector containing the forced frequencies for the healthy case, $\{f^*_{unk}\}$ is a vector containing the forced frequencies for an unknown-health case, and $\{f^*_{diff}\}$ is a vector containing the differences between $\{f^*_{unk}\}$ and $\{f^*_h\}$.

Once the vector $\{f^*_{diff}\}$ is calculated, it is then compared to the database of stored vectors $\{f^i_{diff}\}$ from eigenvalue analysis. Therefore, the objective function, O^i, can be defined by Equation (3). Those vectors from eigenvalue analysis leading to a minimum value of the objective function are used to estimate the damage severity and location.

$$O^i = \left\{\{f^*_{diff}\} - \{f^i_{diff}\}\right\}^T \cdot \left\{\{f^*_{diff}\} - \{f^i_{diff}\}\right\} \tag{3}$$

where *T* is the symbol for vector transpose.

There could be cases with two or more potential solutions (i.e., two local minima) due to the symmetrical nature of the frequency changes that has been highlighted before. A second parameter VS^i, defined by Equation (4), is calculated to assess the similarity of vectors $\{f^*_{diff}\}$ and $\{f^i_{diff}\}$, and to discern the true solution amongst several candidates corresponding to the lowest values of the objective function. VS^i is based on the modal assurance criterion, which is a statistical indicator very sensitive to differences between two vectors. VS^i has values laying between 0 and 1, where 1 represents fully consistent vectors and 0 indicates that those vectors are not consistent. The candidate solution with the highest value of VS^i will be selected as the true damage location. It must be noted that VS^i is a useful tool for locating damage in case of uncertainty, but the quantification of damage is carried out more accurately by the objective function O^i.

$$VS^i = \frac{\left(\{f^*_{diff}\}^T \cdot \{f^i_{diff}\}\right)^2}{\left(\{f^*_{diff}\}^T \cdot \{f^*_{diff}\}\right) \times \left(\{f^i_{diff}\}^T \cdot \{f^i_{diff}\}\right)} \tag{4}$$

4 THEORETICAL TESTING

4.1 *Scenario 1: 10% damage located at 7 m*

Figure 8 plots the vector $\{f^*_{diff}\}$ of differences between forced frequencies versus vehicle position in the healthy condition and another 'unknown-health status', obtained using STFT. These differences vary between 0.126 Hz and 0.140 Hz depending on the vehicle position from the first support.

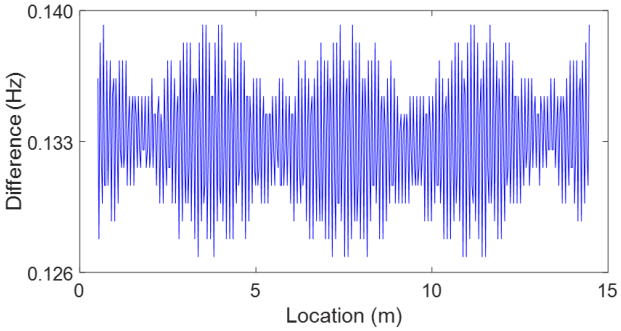

Figure 8. Change in forced frequencies for different positions of the vehicle between a healthy beam and a beam with 10% damage at 7 m from first support.

Figure 9 is a bar plot (plan view) of the values of the objective function O^i (Equation (3)) corresponding to each combination i of damage location and severity considered in eigenvalue analysis. The visualization of a minimum in the figure is not clear due to a scale problem derived from the wide range of values adopted by the objective function. The highest values are highlighted in bright yellow, i.e., combinations of high damage severity (20%, 25%, 30%) and locations near mid-span (at 6, 7, 8 and 9 m from the first support) are discarded as potential solutions. The smallest values are highlighted in dark blue. The lighter blue colour is found for lower damage severity (0%, 5%, 10%) near the two supports (2, 3, 12, and 13 m from the first support) where damage is also discarded. Therefore, it is necessary to zoom into the smallest values denoted by dark blue to distinguish the global minimum.

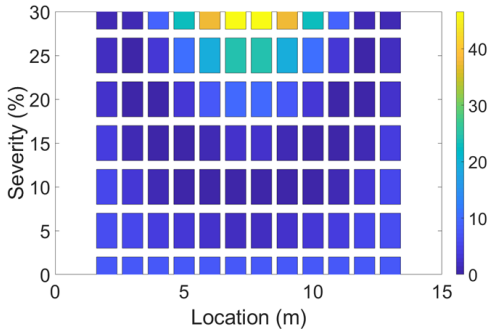

Figure 9. Bar plot of the objective function for scenario 1: 10% damage located at 7 m.

Figure 10 shows the local minima of the objective function for each possible location of damage. Each point in the graph is associated with a damage location (x-axis) and severity (numerical label beside each point). Two solutions symmetrically located with respect to midspan yield the lowest values of the objective function: 10% damage located at 7 m and 10% damage at 8 m.

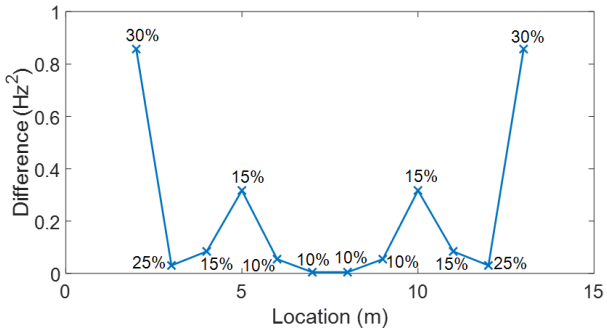

Figure 10. Minimum values of the objective function versus damage location for case 1: 10% damage located at 7 m.

Here, the VS^i parameter (Equation (4)) is used to resolve the uncertainty about the location. Figure 11 gives a contour plot of VS^i values versus damage severity and location. As expected, there is a loss of sensitivity with respect to damage severity compared to Figure 9, but the location is more accurately defined than in Figure 10. The highest values of VS^i are highlighted in bright yellow. A higher value of VS^i represents a larger similarity in shapes between vectors $\{f^*_{diff}\}$ and $\{f^i_{diff}\}$. The maximum is denoted by a red dashed vertical line at 7 m, which allows to successfully conclude that the beam experiences a 10% damage located at 7 m.

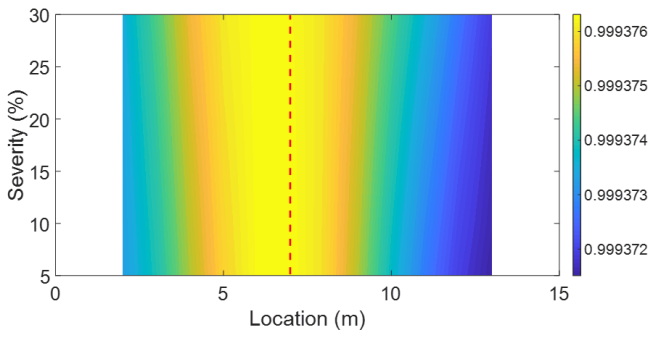

Figure 11. Contour plot of VS^i values for scenario 1: 10% damage located at 7 m.

4.2 *Scenario 2: 25% damage located at 2 m*

Figure 12 shows the vector $\{f^*_{diff}\}$ of differences between forced frequencies in the healthy condition and another 'unknown-health status' for the second scenario under investigation. The values in the y-

axis vary between 0.064 Hz and 0.076 Hz depending on the vehicle position. This range of variation in forced frequency is approximately half the width of the frequency range observed in Figure 8 for scenario 1.

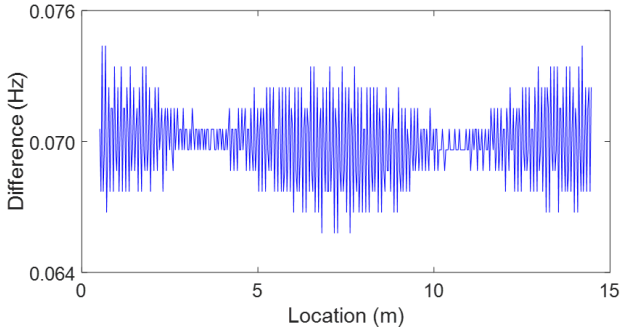

Figure 12. Change in forced frequencies for different positions of the vehicle between a healthy beam and a beam with 25% damage at 2 m from first support.

Figure 13 shows a bar plot (plan view) of the objective function. As before, the highest and smallest values are highlighted in bright yellow and dark blue, respectively. While this figure allows quickly identifying regions where damage will not be present, the global minimum is located somewhere in a vast region that is difficult to visualize due to the large difference between the maximal and minimal values adopted by the objective function.

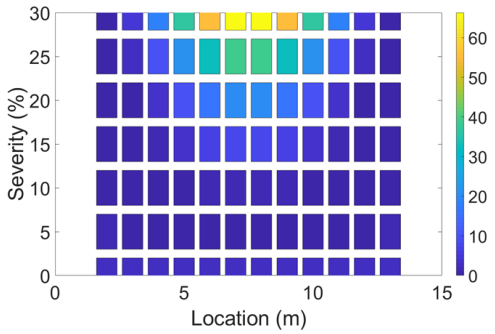

Figure 13. Bar plot of objective function for scenario 2: 25% damage located at 2 m.

As for scenario 1, a total of 12 values of the objective function, one per damage location, are plotted in Figure 14. These 12 values correspond to the damage severity giving the lowest value of the objective function for the location of damage indicated by the *x*-axis. Again, apparently two symmetric solutions with respect to midspan are possible: 25% damage located at 2 m from the first support and 25% damage located at 13 m from the first support.

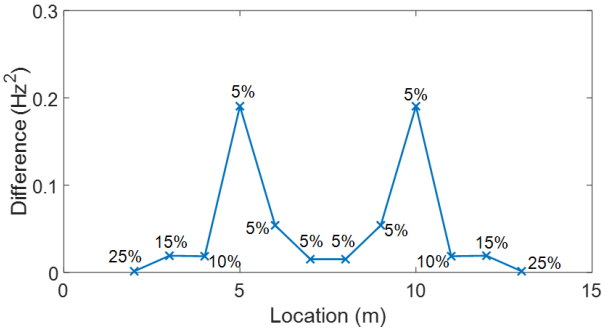

Figure 14. Minimum values of the objective function versus damage location for scenario 2: 25% damage located at 2 m.

Figure 15 gives the value of the VS^i parameter versus damage severity and location. The maximum value of VS^i (i.e., maximal similitude of shapes) is located at 2 m. The latter is signalled by a vertical red dashed line. Therefore, the method correctly estimates that the answer is 25% damage located at 2 m from the first support, as opposed to 25% damage at 13 m from the first support.

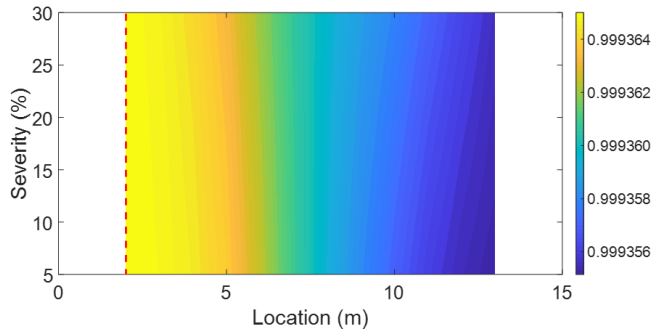

Figure 15. Contour plot of VS^i values for scenario 2: 25% damage located at 2 m.

5 CONCLUSIONS

A model-based SHM method has been proposed for locating and quantifying damage in a bridge from forced frequencies due to a moving vehicle. Using eigenvalue analysis and simplified vehicle and bridge models, it has been shown that there are changes in magnitude and curvature when computing differences between forced frequencies in healthy and damaged conditions. These changes also appear in the instantaneous forced frequencies derived from applying the STFT to the transient response. It has been demonstrated how stiffness loss can be located and quantified from comparing transient analysis results to eigenvalue analysis via an objective function. Cases when more than one solution is possible, i.e., due to symmetry in the frequency response, have been resolved through a parameter that quantifies the similarity between the shapes of the time history of forced frequencies by eigenvalue

and transient analyses. Although preliminary results in this paper are promising, they have been based on a quarter-car crossing a simply supported beam, and further validation involving more complex models, higher speeds, road profile, noise, slight variations in vehicle properties, and experimental data is needed.

6 ACKNOWLEDGEMENTS

This research has received funding from Science Foundation Ireland (SFI)'s US-Ireland R&D partnership programme under the proposal id. 16/US/I3277 titled MARS-Fly.

7 REFERENCES

Amezquita-Sanchez, J.P. & Adeli, H. 2016. Signal processing techniques for vibration-based health monitoring of smart structures. *Archives of Computational Methods in Engineering* 23(1): 1-15.

Cantero, D. & González, A. 2008. Location and evaluation of maximum dynamic effects on a simply supported beam due to a quarter-car model. *Bridge and Infrastructure Research In Ireland (BRI 2008), December, 2008.* Galway, Ireland.

Cantero, D., Hester, D. & Brownjohn, J. 2017. Evolution of bridge frequencies and modes of vibration during truck passage. *Engineering Structures* 152: 452-464.

Cantero, D. & OBrien, E.J. 2013. The non-stationarity of apparent bridge natural frequencies during vehicle crossing events. *FME transactions* 41(4): 279-284.

Chang, K., Kim, C. & Borjigin, S. 2014. Variability in bridge frequency induced by a parked vehicle. *Proceedings of the 4th KKCNN Symposium on Civil Engineering*.

Fan, W. & Qiao, P. 2011. Vibration-based damage identification methods: a review and comparative study. *Structural health monitoring* 10(1): 83-111.

Frýba, L. 1972. Vibration of solids and structures under moving loads, *Springer Science & Business Media*.

Gkoumas, K., Marques Dos Santos, F., Van Balen, M., Tsakalidis, A., Ortega Hortelano, A., Grosso, M., Haq, G. & Pekár F. 2019. Research and Innovation in Bridge Maintenance, *Inspection and Monitoring*.

González, A. 2010. Vehicle-bridge dynamic interaction using finite element modelling. *Finite element analysis, IntechOpen*.

González, A., Casero, M. & Feng, K. 2020. Sensitivity to Damage of the Forced Frequencies of a Simply Supported Beam Subjected to a Moving Quarter-Car. *Lecture Notes in Mechanical Engineering*: 350-362.

Guan, H., Karbhari, V.M. & Sikorsky, C.S. 2006. Web-based structural health monitoring of an FRP composite bridge. *Computer-Aided Civil and Infrastructure Engineering* 21(1): 39-56.

Lederman, G., Wang, Z., Bielak, J., Noh, H., Garrett, J., Chen, S., Kovacevic, J., Cerda, F. & Rizzo, P. 2014. Damage quantification and localization algorithms for indirect SHM of bridges. *Proc. Int. Conf. Bridge Maint., Safety Manag.*, Shanghai, China.

Sinha, J.K., Friswell, M. & Edwards, S. 2002. Simplified models for the location of cracks in beam structures using measured vibration data. *Journal of Sound and vibration* 251(1): 13-38.

Sun, Z. & Chang, C.C. 2002. Structural damage assessment based on wavelet packet transform. *Journal of structural engineering* 128(10): 1354-1361.

Yang, Y., Dorn, C., Mancini, T., Talken, Z., Theiler, J., Kenyon, G., Farrar, C. & Mascarenas, D. 2018. Reference-free detection of minute, non-visible, damage using full-field, high-resolution mode shapes output-only identified from digital videos of structures. *Structural Health Monitoring* 17(3): 514-531.